Journal of Solid State Chemistry 184 (2011) 470–475

Contents lists available at ScienceDirect

Journal of Solid State Chemistry

journal homepage: www.elsevier.com/locate/jssc

A comparison of the transport properties of lithium-stuffed garnets and the conventional phases $Li_3Ln_3Te_2O_{12}$

Edmund J. Cussen *, Thomas W.S. Yip, Gemma O'Neill, Michael P. O'Callaghan [1]

WestCHEM, Department of Pure and Applied Chemistry, University of Strathclyde, Thomas Graham Building, 295 Cathedral Street, Glasgow G1 1XL, UK

ARTICLE INFO

Article history:
Received 6 September 2010
Received in revised form
15 December 2010
Accepted 21 December 2010
Available online 29 December 2010

Keywords:
Ionic conduction
Lithium
Garnet
Crystallography
Diffraction

ABSTRACT

The structures of new phases $Li_6CaLa_2Sb_2O_{12}$ and $Li_{6.4}Ca_{1.4}La_2Sb_2O_{12}$ have been characterised using neutron powder diffraction. Rietveld analyses show that both compounds crystallise in the space group $la\bar{3}d$ and contain the lithium cations in a complex arrangement with occupational disorder across oxide tetrahedra and distorted oxide octahedra, with considerable positional disorder in the latter. Variable temperature neutron diffraction experiments on $Li_{6.4}Ca_{1.4}La_2Sb_2O_{12}$ show the structure is largely invariant with only a small variation in the lithium distribution as a function of temperature. Impedance spectroscopy measurements show that the total conductivity of $Li_6CaLa_2Sb_2O_{12}$ is several orders of magnitude smaller than related lithium-stuffed garnets with $\sigma = 10^{-7}$ S cm^{-1} at 95 °C and an activation energy of 0.82(3) eV. The transport properties of the conventional garnets $Li_3Gd_3Te_2O_{12}$, $Li_3Tb_3Te_2O_{12}$, $Li_3Er_3Te_2O_{12}$ and $Li_3Lu_3Te_2O_{12}$ have been evaluated and consistently show much lower values of conductivity, $\sigma \leq 4.4 \times 10^{-6}$ S cm^{-1} at 285 °C and activation energies in the range $0.77(4) \leq E_a/\text{eV} \leq 1.21(3)$.

1. Introduction

The garnet structure is capable of incorporating a wide range of cations due to the presence of three different, geometrically regular coordination environments; in the classical $A_3B_3C_2O_{12}$ stoichiometry A is eight coordinate, B is tetrahedrally coordinated and C is in an octahedral site. These key features of the garnet structure are illustrated in Fig. 1. There has recently been a resurgence of interest in this structure due to the observation of fast lithium ion conduction in a number of phases containing an excess of lithium that surpasses the above stoichiometry [1,2]. These lithium-stuffed garnets house the lithium in a mixture of the tetrahedrally coordinated B site and in a large, heavily distorted octahedron that is vacant in the classical $A_3B_3C_2O_{12}$ compounds. There is considerable positional and occupational disorder in the fast-ion conducting phases [3,4] and the conductivity shows a general increase with lithium content [5] until for compositions such as $Li_7La_3Sn_2O_{12}$ lithium cation ordering occurs and the conductivity is drastically reduced compared to the disordered phases [6,7].

These compounds have attracted interest for applications as solid state electrolytes because in addition to showing fast lithium ion conduction they have two other key attributes: (i) several compositions, mainly including Ta^{5+}, are highly resistant to reduction and so do not react with elemental lithium or other highly reduced cathode materials; (ii) the grain boundary resistance for some of these phases is not significantly larger than the intra-grain resistance and so bulk transport through the electrolyte is facile. For most compounds it has not been possible to evaluate fully the intra- and inter-grain contributions to the conductivity for all temperatures. However as these two contributions have been seen to be approximately equal, the total conductivity as determined by impedance analysis has been used as surrogate data to prove the mechanism for transport of Li^+ through the crystal lattice.

Here we present two new lithium stuffed garnets based on Sb^{5+} and doped with Ca^{2+}. A number of Sb^{5+} based garnets have been studied before and these have shown conductivity behaviour [8,9] that has been in reasonable agreement with that observed from other lithium-stuffed garnets, as could be anticipated by similarities in the structure of compounds based on Sb^{5+}, Ta^{5+} or Nb^{5+} [8,10,11]. The transport properties of $Li_6CaLa_2Sb_2O_{12}$ that we report here show considerable differences from previous reports of similar lithium-stuffed garnets. In light of this we have carried out a series of transport measurements on garnets that follow the conventional stoichiometry that have previously been structurally characterised [12].

2. Experimental

Antimony based phases were prepared by grinding together stoichiometric quantities of calcium carbonate, strontium

* Corresponding author. Fax: +44 141 548 4822.
E-mail address: Edmund.Cussen@Strath.ac.uk (E.J. Cussen).
[1] Present address: Dstl Porton Down, Salisbury, Wiltshire SP4 0JQ, UK.

0022-4596/$ - see front matter © 2010 Elsevier Inc. All rights reserved.
doi:10.1016/j.jssc.2010.12.021

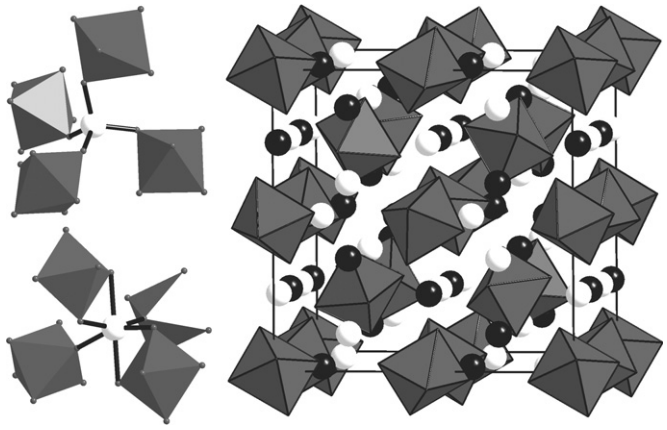

Fig. 1. The crystal structure of the garnet $Li_5La_3Ta_2O_{12}$ contains 8-coordinate La and TaO_6 units shown as black spheres and octahedra, respectively. Lithium is shown as light spheres and is accommodated in a mixture of regular oxide tetrahedra and heavily distorted octahedra [3].

carbonate, lanthanum oxide and antimony (V) oxide with a 10% excess of lithium hydroxide monohydrate in an agate mortar and pestle. This mixture was pressed into a pellet of 13 mm diameter and heated from room temperature to 700 °C at 1 °C min^{-1} and held at this temperature for 12 h. The pellet was then ground and re-pressed before heating from 700 to 900 °C at 2.5 °C min^{-1} and heating at this temperature for 24 h. This second stage was repeated until the X-ray diffraction pattern of the resultant materials could be fully indexed as a single garnet phase. All tellurium and tungsten based compounds were prepared in a similar manner as described previously [12].

X-ray diffraction data were collected from these polycrystalline samples using a Siemens D500 diffractometer operating in Bragg Brentano geometry using Cu $K\alpha$ radiation. Data suitable for Rietveld analysis were collected over the range $8 \leq 2\theta/^\circ \leq 100$ with a step size of $2\theta = 0.02^\circ$. Neutron powder diffraction data were collected using the time-of-flight Polaris instrument at the ISIS neutron facility at Rutherford Appleton Laboratories. Diffraction data were analysed using the Rietveld method [13] of structure refinement as implemented in the GSAS suite of programs.[14] The background was modelled using a shifted Chebyshev function and the X-ray diffraction peak shape was modelled using a pseudo-Voigt function. The neutron diffraction peak shape was modelled using a convolution of exponential and pseudo-Voigt functions and the structural refinements were carried out against neutron data collected from all three banks simultaneously.

Impedance measurements were carried out on cylindrical sample pellets of 13 mm diameter and 3–4 mm thickness that had been formed by pressing at room temperature under a load of 1 tonne for 2–3 min. These pellets were sintered at 600 °C for *ca.* 3 h prior to the application of platinum paste to opposing faces of the pellet to make electrical contacts. Data were collected isothermally on both heating and cooling and the temperature of the system was allowed to equilibrate for at least 1 h before every data collection. Data were collected using a Solartron 1260 impedance analyser and were analysed using the ZView2 software package.

3. Results

3.1. Structural study

The two title compounds yielded X-ray diffraction patterns that could be fully indexed using cubic unit cells with the space group symmetry $la\bar{3}d$. As has been noted in related phases it was not possible to determine the lithium distribution in these phases due to the dominant effect of scattering from La^{3+} and Sb^{5+}. Consequently the structures of these compounds were refined against time-of-flight neutron diffraction data. In addition to the peaks allowed by the garnet phase the patterns contained a number of additional Bragg peaks arising from the vanadium sample container and small quantities of lithium carbonate impurity. The latter was typically present at levels, of no more than 0.5 wt%, that are undetectable in the X-ray diffraction data.

In all cases the refinement proceeded by using structures from the compositional series $Li_{5+x}Ba_xLa_{3-x}Ta_2O_{12}$ as starting models albeit with the lattice parameters adjusted to smaller values to reflect the smaller ion radius of Ca^{2+} compared to Ba^{2+} [4]. All of the peaks could be indexed in a straightforward manner with no evidence of either a tetragonal distortion that has been observed for compositions $Li_7La_3M_2O_{12}$ (M=Zr, Sn) [6,7] or the peak asymmetry arising from a mixture of garnet phases seen in samples of $Li_5Nd_3Sb_2O_{12}$ [8]. The structural model was refined in a straightforward manner. The eight-coordinate cations, i.e. La^{3+} and Ca^{2+} were placed on the same crystallographic special position which has no positional degrees of freedom, and the displacement parameters were constrained to take the same value. The displacement parameters of all non-lithium species were allowed to vary anisotropically, within the constraints of the point symmetry of the site. The parameters associated with the displacement of Sb^{5+} and position and displacement of the oxide anions refined readily to convergence. There was no evidence of oxide vacancies in any of these samples and all anisotropic displacement parameters showed largely spherical distributions of scattering. The arrangement of lithium cations in this model is complex and involves considerable positional and occupational disorder that is modelled using split sites and isotropic displacement parameters. All compounds contain lithium in the single site inside the oxide tetrahedra occupied for garnets with conventional stoichiometries. The additional lithium is found in a disordered arrangement across two crystallographically distinct sites inside the distorted octahedra. In all four compounds it was necessary to include lithium on both the central (48*g*) and displaced (96*h*) positions in the octahedra in order to achieve a satisfactory fit to the diffraction profile. The displacement parameters of these two sites were constrained to the same isotropic value. All attempts to use a simpler lithium distribution, i.e. with only one crystallographic site occupied in the oxide octahedra, resulted in significant mismatch between the observed and calculated profiles. The additional data sets collected from $Li_{6.4}Ca_{1.4}La_{1.6}Sb_2O_{12}$ were fitted using the same structural model. Data were collected from $Li_{6.4}Ca_{1.4}La_{1.6}Sb_2O_{12}$ at 2 K for 50% longer than at the other temperatures and this is responsible for the anomalously high χ^2 value for the structural refinement against these data. Representative fits are shown in Fig. 2 and the lattice parameters, atomic parameters, displacement parameters and key interatomic distances are collected in Tables 1–4, respectively.

3.2. Transport measurements

The impedance data collected from $Li_6CaLa_2Sb_2O_{12}$ showed a single semicircular arc in the temperature range of $200 \leq T/^\circ C \leq 375$ and a linear tail at low frequency that is indicative of ion blocking. At lower temperatures it was possible to detect two contributions to the impedance, although even in data which provided the clearest evidence of two arcs, collected at 125 °C, the extensive overlap meant that resolution of the different contributions was problematic. Nevertheless, the presence of a much

smaller arc associated with a smaller capacitance at higher frequencies has been reported in related garnets and has been clearly identified as arising from intra-grain conductivity. If the same assignment is made here it suggests that the values for intra-grain conductivity are typically an order of magnitude higher than that of the total conductivity, i.e. the sum of the intra- and inter-grain conductivity, with an intra-grain conductivity at 95 °C of 10^{-7} S cm^{-1}. At temperatures lower than 95 °C the total impedance of the system was too large to reliably extract a value for the conductivity. Data collected at 400 °C and above showed that the impedance of the pellet had fallen to such a low value that the arc had moved beyond the high frequency detection limit of the instrument. Representative impedance data displaying two and one semicircles, collected at 125 and 350 °C, respectively, are plotted in the complex plane in Fig. 3.

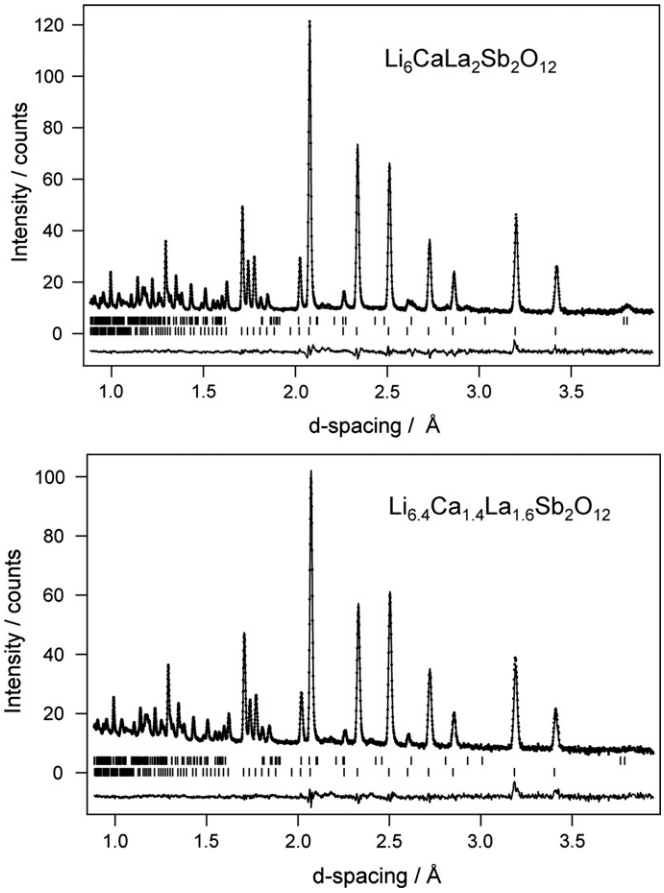

Fig. 2. Neutron powder diffraction patterns collected from $Li_6CaLa_2Sb_2O_{12}$ and $Li_{6.4}Ca_{1.4}La_{1.6}Sb_2O_{12}$ at room temperature. The mismatch between the observed (dots) and calculated data (line) is illustrated by the difference curve. Allowed Bragg reflections are corresponding to the garnet (lower marks) and lithium carbonate (upper marks) are indicated.

As it is not possible to reliably extract intra-grain conductivity over an extended temperature range the data were analysed to give a value of the total impedance that can be compared usefully with total conductivities reported in the literature [1,15]. The total conductivity displays an Arrhenius temperature dependence as shown in Fig. 4, with an activation energy of 0.82(3) eV and a total conductivity of 10^{-8} S cm^{-1} at 95 °C and 6×10^{-4} S cm^{-1} at 375 °C.

As $Li_6CaLa_2Sb_2O_{12}$ showed substantially lower conductivity than many previously reported Li-stuffed garnets it was decided to re-investigate the properties of stoichiometric garnets. Impedance data were also collected from various compounds in the series $Li_3Ln_3Te_2O_{12}$ (Ln=Gd, Tb, Er, Lu). These compounds were prepared as reported previously [12] and X-ray diffraction data showed them to be single phase samples. All of these compounds showed greatly reduced conductivity that was immeasurably small at temperatures below 280 °C, for $Li_3Tb_2Te_2O_{12}$, and *ca.* 425 °C for the other compounds. All impedance data collected from these compounds showed a single arc in the complex plane and so it was not possible to determine inter- and intra-grain contributions to the conductivity. At 480 °C the data collected from $Li_3Tb_2Te_2O_{12}$ no longer displayed a substantial response from the pellet, but was dominated by the blocking effect of the electrodes. Data were collected from the other three compositions at temperatures up to 600 °C. In all cases the data were analysed using an equivalent circuit of a resistor in parallel with a constant phase element to model the total impedance of the sample pellet. The total conductivities derived from these fits are displayed in Fig. 5 and show that the data from $Li_3Tb_3Te_2O_{12}$ show a pronounced non-linearity, whilst data from the other compounds show a well-defined Arrhenius dependence on temperature. Activation energies for these compounds span the range 0.88(3) eV, for $Li_3Gd_3Te_2O_{12}$, to 1.21(3) eV, for $Li_3Er_3Te_2O_{12}$ and are collected along with other transport properties in Table 5. Carrying out a linear fit to the data obtained from $Li_3Tb_3Te_2O_{12}$ gives an approximate value for activation energy of 0.77(4) eV.

4. Discussion

The structures of $Li_6CaLa_2Sb_2O_{12}$ and $Li_{6.4}Ca_{1.4}La_{1.6}Sb_2O_{12}$ are largely similar to those observed in other lithium-stuffed cubic garnets. The complex lithium distribution across multiple sites within the oxide octahedron as well as the tetrahedron has been consistently reported for the related Sr^{2+} phases [11,16] as well as the series $Li_{5+x}Ba_xLa_2Ta_2O_{12}$ [4]. At higher lithium contents it is known that Li^+-ordering can occur [6,7], and extremely high-resolution neutron diffraction data have revealed possible two-phase behaviour [8]. However, neither effect was evident in any of the data collected from the present compounds. As would be anticipated, the replacement of Ba^{2+} with Ca^{2+} leads to a reduction in the lattice parameters when comparing e.g. $Li_6CaLa_2Sb_2O_{12}$ with $Li_6BaLa_2Ta_2O_{12}$ [4]. However, the observed reduction in lattice parameter, of 1.8%, is less than would be anticipated purely

Table 1
Fit parameters and lithium site occupancy for $Li_6CaLa_2Sb_2O_{12}$ and $Li_{6.4}Ca_{1.4}La_{1.6}Sb_2O_{12}$ derived from Rietveld refinement against neutron powder diffraction data.

Compound	a_o/Å	R_{wp}	χ^2	24*d* occupancy	48*g* occupancy	96*h* occupancy
$Li_6CaLa_2Sb_2O_{12}$	12.78594(12)	2.09	2.751	0.665(6)	0.270(13)	0.199(5)
$Li_{6.4}Ca_{1.4}La_{1.6}Sb_2O_{12}$—2 K	12.7622(2)	2.57	8.767	0.523(9)	0.289(13)	0.258(4)
$Li_{6.4}Ca_{1.4}La_{1.6}Sb_2O_{12}$—RT	12.7730(2)	2.21	4.793	0.565(10)	0.29(2)	0.245(6)
$Li_{6.4}Ca_{1.4}La_{1.6}Sb_2O_{12}$—473 K	12.8036(2)	2.06	4.157	0.558(11)	0.30(2)	0.242(8)
$Li_{6.4}Ca_{1.4}La_{1.6}Sb_2O_{12}$—673 K	12.8522(2)	1.99	3.652	0.509(11)	0.34(2)	0.236(8)
$Li_{6.4}Ca_{1.4}La_{1.6}Sb_2O_{12}$—873 K	12.8989(2)	1.86	3.136	0.528(14)	0.38(2)	0.210(8)

Table 2
Structural information for $Li_6CaLa_2Sb_2O_{12}$ and $Li_{6.4}Ca_{1.4}La_{1.6}Sb_2O_{12}$ derived from neutron powder diffraction data.

Compound	Li (48*g*)		Li (96*h*)			O (96*h*)		
	y	*z*	*x*	*y*	*z*	*x*	*y*	*z*
$Li_6CaLa_2Sb_2O_{12}$	0.6772(4)	0.5728(4)	0.0914(7)	0.6918(6)	0.5773(5)	0.28057(3)	0.10527(3)	0.20139(3)
$Li_{6.4}Ca_{1.4}La_{1.6}Sb_2O_{12}$—2 K	0.6800(4)	0.5700(4)	0.0902(5)	0.6930(4)	0.5750(4)	0.28087(5)	0.10457(4)	0.20233(4)
$Li_{6.4}Ca_{1.4}La_{1.6}Sb_2O_{12}$—RT	0.6796(5)	0.5705(5)	0.0908(7)	0.6933(7)	0.5779(5)	0.28090(5)	0.10480(5)	0.20221(5)
$Li_{6.4}Ca_{1.4}La_{1.6}Sb_2O_{12}$—473 K	0.6794(6)	0.5706(6)	0.0908(9)	0.6936(8)	0.5795(6)	0.28072(5)	0.10497(5)	0.20246(5)
$Li_{6.4}Ca_{1.4}La_{1.6}Sb_2O_{12}$—673 K	0.6803(6)	0.5697(6)	0.0897(10)	0.6940(8)	0.5799(8)	0.28044(5)	0.10494(4)	0.20325(5)
$Li_{6.4}Ca_{1.4}La_{1.6}Sb_2O_{12}$—873 K	0.6799(5)	0.5701(5)	0.0884(12)	0.6950(10)	0.5802(8)	0.28012(5)	0.10507(5)	0.20366(5)

Atomic coordinates: La/Ca 24*c* $^1/_8$, 0, $^1/_4$; Sb 16*a* 0, 0, 0; Li 24*d* $^1/_4$, $^7/_8$, 0; Li 48*g* $^1/_8$, *y*, *z*; Li 96*h* *x*, *y*, *z*.

Table 3
Displacement parameters (Å^2) for $Li_6CaLa_2Sb_2O_{12}$ and $Li_{6.4}Ca_{1.4}La_{1.6}Sb_2O_{12}$ derived from neutron powder diffraction data.

Compound	Li (24*d*)	Li (48*g*)[a]	Sb[b]		La/Ca[c]			O					
	$100U_{iso}$	$100U_{iso}$	$100U_{11}$	$100U_{12}$	$100U_{11}$	$100U_{22}$	$100U_{23}$	$100U_{11}$	$100U_{22}$	$100U_{33}$	$100U_{12}$	$100U_{13}$	$100U_{23}$
$Li_6CaLa_2Sb_2O_{12}$	4.25(12)	1.91(10)	0.785(13)	0.06(2)	1.69(4)	1.05(2)	0.38(2)	1.90(2)	1.10(2)	1.81(2)	−0.08(2)	−0.14(2)	−0.29(2)
$Li_{6.4}Ca_{1.4}La_{1.6}Sb_2O_{12}$ 2 K	4.5(2)	0.35(7)	0.66(2)	0.28(3)	1.33(5)	0.65(2)	0.34(3)	1.70(3)	0.93(3)	1.40(3)	0.07(2)	−0.08(2)	−0.15(2)
$Li_{6.4}Ca_{1.4}La_{1.6}Sb_2O_{12}$ RT	5.9(3)	1.30(12)	0.94(2)	0.24(3)	1.45(6)	1.15(3)	0.37(4)	2.06(4)	1.09(3)	1.79(4)	0.14(3)	−0.07(3)	−0.20(3)
$Li_{6.4}Ca_{1.4}La_{1.6}Sb_2O_{12}$ 473 K	7.3(4)	2.07(14)	1.19(3)	0.30(4)	1.58(6)	1.53(3)	0.49(4)	2.39(4)	1.34(3)	2.29(4)	0.23(3)	−0.02(3)	−0.17(3)
$Li_{6.4}Ca_{1.4}La_{1.6}Sb_2O_{12}$ 673 K	8.1(5)	2.66(15)	1.39(3)	0.21(4)	1.57(6)	1.87(4)	0.41(4)	2.74(4)	1.56(3)	2.84(5)	0.27(3)	0.16(3)	−0.18(3)
$Li_{6.4}Ca_{1.4}La_{1.6}Sb_2O_{12}$ 873 K	10.8(6)	3.1(2)	1.63(3)	0.15(4)	1.90(7)	2.26(4)	0.44(4)	3.12(5)	1.93(4)	3.62(5)	0.27(3)	0.32(3)	−0.22(3)

[a] U_{iso} Li (48*g*)=U_{iso} Li (96*h*), the displacement parameter of Li(96*h*) was constrained to the same value as Li(48*g*).
[b] $U_{33}=U_{22}=U_{11}$, $U_{13}=U_{23}=U_{12}$.
[c] $U_{33}=U_{22}$, $U_{12}=U_{13}=0$.

Table 4
Selected bond distances (Å) and angles (°) for $Li_6CaLa_2Sb_2O_{12}$ and $Li_{6.4}Ca_{1.4}La_{1.6}Sb_2O_{12}$ derived from neutron powder diffraction data.

Compound	*A*–O–*A* angle/deg.	Bond distance/Å									
		A–O × 4	*A*–O × 4	Sb–O	Li(24*d*)–O	Li(24*d*)–Li(48*g*)	Li(24*d*)–Li(96*h*)	Li(24*d*)–Li(96*h*)	Li(48*g*)–O × 2	Li(48*g*)–O × 2	Li(48*g*)–O × 2
$Li_6CaLa_2Sb_2O_{12}$	100.32(1)	2.4808(4)	2.6166(4)	1.9909(4)	1.9120(4)	1.9662(7)	1.514(9)	2.412(9)	1.917(4)	2.3219(5)	2.535(6)
$Li_{6.4}Ca_{1.4}La_{1.6}Sb_2O_{12}$—2 K	100.08(2)	2.4715(6)	2.6250(6)	1.9925(5)	1.8959(5)	1.9585(5)	1.504(6)	2.414(6)	1.942(4)	2.3022(6)	2.487(5)
$Li_{6.4}Ca_{1.4}La_{1.6}Sb_2O_{12}$—RT	100.07(2)	2.4758(6)	2.6255(6)	1.9920(5)	1.8998(6)	1.9607(7)	1.494(9)	2.426(10)	1.938(6)	2.3063(7)	2.498(7)
$Li_{6.4}Ca_{1.4}La_{1.6}Sb_2O_{12}$—473 K	100.04(2)	2.4803(6)	2.6344(6)	1.9934(6)	1.9063(6)	1.9656(8)	1.487(12)	2.442(12)	1.943(6)	2.3097(7)	2.509(8)
$Li_{6.4}Ca_{1.4}La_{1.6}Sb_2O_{12}$—673 K	99.92(2)	2.4841(6)	2.6539(6)	1.9975(6)	1.9123(6)	1.9720(7)	1.477(13)	2.467(13)	1.965(6)	2.3091(7)	2.511(8)
$Li_{6.4}Ca_{1.4}La_{1.6}Sb_2O_{12}$—873 K	99.90(2)	2.4895(7)	2.6679(7)	2.0008(6)	1.9214(6)	1.9795(7)	1.46(2)	2.50(2)	1.973(5)	2.3139(7)	2.529(7)

on the basis of changes in ionic radii. The $Ba(Ca)O_8$ units are linked *via* edges to form a continuous body-centred cubic lattice. Ba^{2+} and O^{2-} have similar radii and so a reduction in the mean radius of the eight-coordinate cations of 8.0% on replacing Ba^{2+} with Ca^{2+} would be expected to lead to a reduction in the lattice parameter of *ca.* 4% on changing the composition from $Li_6BaLa_2Ta_2O_{12}$ to $Li_6CaLa_2Sb_2O_{12}$ [17] if the structure was otherwise unchanged. The much smaller contraction in the lattice can be attributed to the increased polarisability of the Sb^{5+}, d^{10}, cation compared to Ta^{5+} with a d^0 configuration. Despite these two species having almost identical radii, the structural behaviour of $Li_6CaLa_2Sb_2O_{12}$ and $Li_{6.4}Ca_{1.4}La_{1.6}Sb_2O_{12}$, taken together with the structures of $Li_5Nd_3Sb_2O_{12}$ [10], $Li_6SrLa_2Sb_2O_{12}$ and $Li_{6.4}Sr_{1.4}La_{1.6}Sb_2O_{12}$ show [11] that replacing Ta^{5+} with Sb^{5+} leads to a significant increase in the unit cell size that is consistent across this range of compositions.

The structure of $Li_{6.4}Ca_{1.4}La_{1.6}Sb_2O_{12}$ shows a small, but significant, change in the distribution of Li^+ as a function of temperature. Previous temperature-dependent structural studies of fast-ion conducting garnets have shown a small reduction in the occupation of the oxide tetrahedra on heating the sample above room temperature [18], and a similar, albeit small, effect is observed in $Li_{6.4}Ca_{1.4}La_{1.6}Sb_2O_{12}$. There is also a significant shift for the population of the lithium in the oxide octahedra from the heavily displaced, 96*h*, positions towards the central 48*g* site. It should be noted that both of these involve changes of only a few percent and so are orders of magnitude smaller than changes in signal intensity that have been reported in some NMR studies of related garnets.[19]

Transport measurements on $Li_6CaLa_2Sb_2O_{12}$ showed an immeasurably large impedance at room temperature and a total conductivity of 10^{-8} S cm^{-1} at 95 °C. The data suggest that the intra-grain conductivity has a higher value of around 10^{-7} S cm^{-1} that is similar to that reported [8] in $Li_5Nd_3Sb_2O_{12}$ (*ca.* 10^{-6} S cm^{-1} at this temperature) but nevertheless $Li_6CaLa_2Sb_2O_{12}$ shows substantially lower total conductivity than $Li_5Nd_3Sb_2O_{12}$ [8] and the related materials $Li_5La_3Sb_2O_{12}$ and $Li_6SrLa_2Sb_2O_{12}$ [9]. A detailed study of the transport properties of $Li_5La_3Sb_2O_{12}$ and $Li_6SrLa_2Sb_2O_{12}$ found that the grain boundary contribution to the total resistance was only

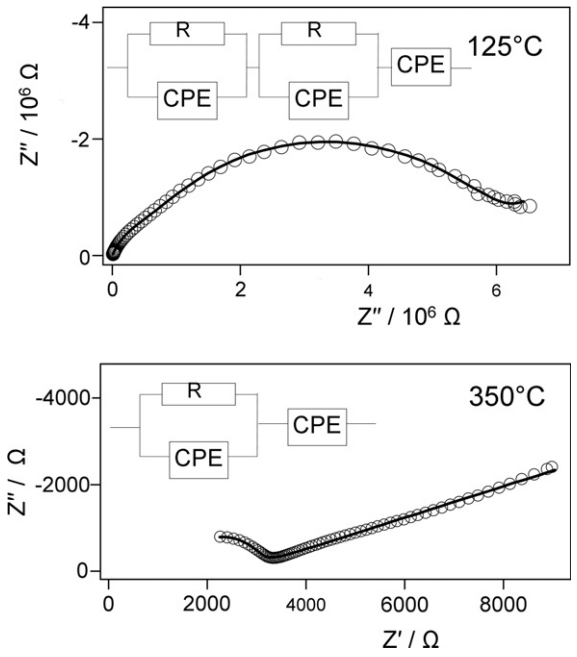

Fig. 3. AC impedance data collected from $Li_6CaLa_2Sb_2O_{12}$ at 125 and 350 °C and plotted in the complex plane. The observed data are represented by circles and the solid line indicates the values calculated using equivalent electrical circuits containing resistors and constant phase elements as shown for each plot.

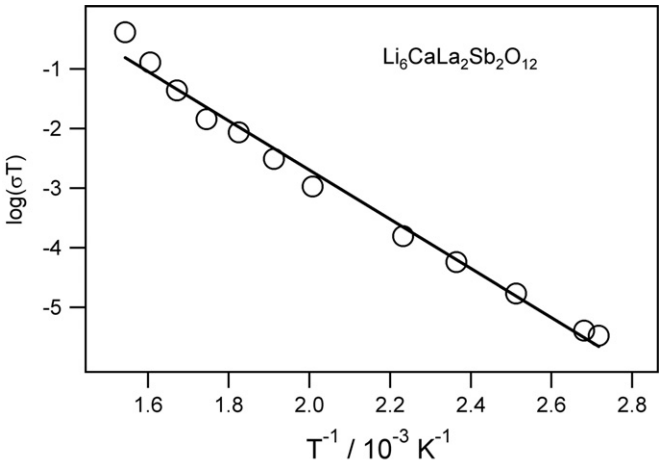

Fig. 4. A plot of conductivity as a function of temperature for $Li_6CaLa_2Sb_2O_{12}$. The line indicates an Arrhenius fit over the whole temperature range.

around 3–5% [9]. This can be contrasted with the measurements on the sample of $Li_6CaLa_2Sb_2O_{12}$ discussed here where the grain boundary appears to be responsible for *ca.* 90% of the total resistance of the sample. These compounds all have very similar compositions and detailed structural analysis of these compounds [11] shows that although there is some evidence for two-phase behaviour in $Li_5La_3Sb_2O_{12}$ the crystal structures are not substantially different; all compounds contain lithium in a mixture of oxide tetrahedra and octahedra, the same space group symmetry, and the other chemical species in the structure are very similar. Consequently it would be anticipated that the transport properties would be broadly similar.

It is probable that the differences in grain boundary conductivity arise from changes in the microstructure of these samples. It is known that such changes can have dramatic effects on transport properties [20] and there are some differences in processing between the different preparations; $Li_5La_3Sb_2O_{12}$ and $Li_6SrLa_2Sb_2O_{12}$ were prepared by extensive ball-milling in 2-propanol and then heated at 950 °C to yield a high density pellet. Similar temperatures were used to sinter a pellet of $Li_5Nd_3Sb_2O_{12}$ that showed a total conductivity of 1.3×10^{-7} S cm^{-1} at room temperature i.e. at least two orders of magnitude higher than observed in $Li_6CaLa_2Sb_2O_{12}$. The pellets of $Li_6CaLa_2Sb_2O_{12}$ used for transport measurements were sintered at 600 °C in order to minimise any structural changes from the samples used for structural studies and this use of a lower temperature is likely to limit particle growth and hence increase the impact of grain boundary resistance on the total conductivity. It is likely that different processing techniques, such as hot-pressing [21], could be used to reduce the microstructural contribution to the total resistivity in this instance. However, the minimal contribution of the intra-grain conductivity reported for many of the garnets suggests that there is little scope for optimising the properties of these samples by adjusting the processing conditions.

As these results suggested that large variations in microstructure are occurring between samples, it was decided to investigate further the transport properties of lithium garnets that follow the conventional $A_3B_3C_2O_{12}$ stoichiometry. Whilst the structures of the series $Li_3Ln_3Te_2O_{12}$ has been thoroughly characterised the transport properties of such compounds has not been widely studied; only one of these compositions has been examined and $Li_3Nd_3Te_2O_{12}$ has been shown to exhibit minimal total conductivity [12]. The conductivities of $Li_3Ln_3Te_2O_{12}$ reported here consistently show lower conductivities that the lithium-stuffed garnets discussed above, albeit with some variation for compounds containing different lanthanides. The highest conductivity, seen in $Li_3Tb_3Te_2O_{12}$, is three orders of magnitude less than the $Li_6CaLa_2Sb_2O_{12}$ at 450 °C, and is immeasurably small at temperatures below 280 °C.

Whilst the other compounds show a straightforward Arrhenuis relationship between conductivity and temperature, $Li_3Tb_3Te_2O_{12}$ shows significant non-linearity. As we are reporting total conductivity it is possible that this complex temperature dependence arises from changes in microstructure. However, these data were collected over multiple heating and cooling cycles and did not show a history dependence. Consequently any microstructural changes induced by heating the pellet must have been reversed on cooling. If the non-linearity arises from changes to the intra-grain impedance then an obvious origin for this behaviour could be a change in the distribution of Li^+ that is responsible for conductivity. Detailed crystallographic studies of the temperature dependence of the structure of both fast-ion conducting garnets, such as $Li_5La_3Ta_2O_{12}$ [3], and $Li_{6.4}Ca_{1.4}La_{1.6}Sb_2O_{12}$ in the present study as well as the conventional garnet $Li_3Nd_3Te_2O_{12}$ [12], have tended to show only small changes in Li^+ distribution. However, the relatively small changes in conductivity necessary to give non-linearity in the conductivity of $Li_3Tb_3Te_2O_{12}$ shown in Fig. 5 could arise from extremely small changes in the lithium distribution that could lie below the sensitivity of diffraction experiments.

Whilst the low conductivities observed here provide qualitative agreement with previous report of minimal ionic mobility in $Li_3Nd_3Te_2O_{12}$, there is considerable variation in the activation energy with the smaller activation energies such as 0.88 eV observed in $Li_3Gd_3Te_2O_{12}$, showing similar values to $Li_6CaLa_2Sb_2O_{12}$. It has been shown that reducing the size of the lanthanide ion reduces the lattice parameter and compresses the oxide tetrahedra around the lithium cation, and so could be anticipated to increase the energy necessary for lithium to leave this site. However, the activation energies presented here, along with the energy of *ca.* 1.3 eV found for $Li_3Nd_3Te_2O_{12}$ [22], do not show a trend with lattice parameter.

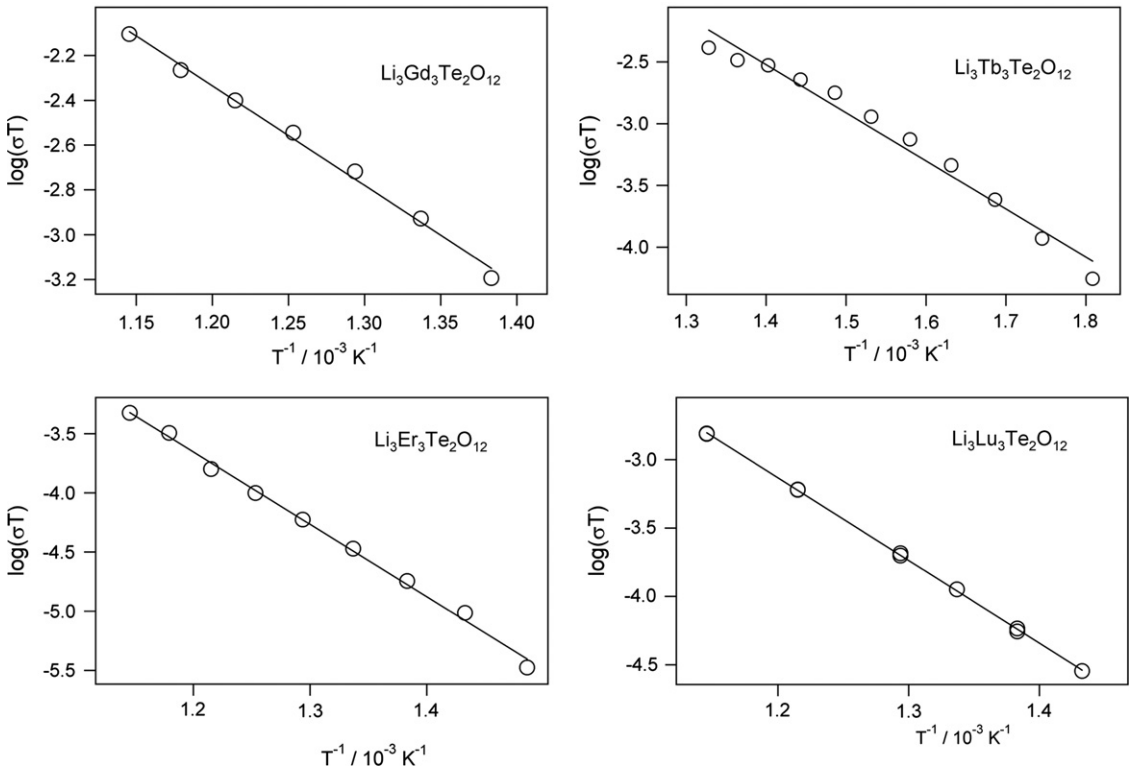

Fig. 5. Arrhenius plots of conductivity for $Li_3Gd_3Te_2O_{12}$, $Li_3Tb_3Te_2O_{12}$, $Li_3Er_3Te_2O_{12}$ and $Li_3Lu_3Te_2O_{12}$. Circles represent values of conductivity derived from impedance spectroscopy data collected over several cycles of heating and cooling.

Table 5
Transport data for $Li_3Ln_3Te_2O_{12}$.

Compound	E_a/eV	$\sigma_{450\ ^\circ C}$/S cm^{-1}
$Li_3Gd_3Te_2O_{12}$	0.88(3)	8.8×10^{-7}
$Li_3Tb_3Te_2O_{12}$	0.77(4)	4.4×10^{-6}
$Li_3Er_3Te_2O_{12}$	1.21(3)	2.8×10^{-8}
$Li_3Lu_3Te_2O_{12}$	1.199(7)	8.1×10^{-8}

5. Conclusions

The lithium-stuffed garnets $Li_6CaLa_2Sb_2O_{12}$ and $Li_{6.4}Ca_{1.4}La_{1.6}Sb_2O_{12}$ accommodate lithium in a complex distribution across oxide tetrahedra and octahedra. The total conductivity of $Li_6CaLa_2Sb_2O_{12}$ is considerably lower than reported for related fast-ion conducting garnets due to a much larger intra-grain contribution to the resistivity than is commonly found for this family of compounds. This suggests that the performance of these compounds shows a greater dependence on sample processing than has previously been acknowledged. The conductivity of several phases that follow the conventional garnet stoichiometry $Li_3Ln_3Te_2O_{12}$ show consistently low lithium mobility indicating that these stoichiometries cannot be considered to provide fast-ion conduction.

Acknowledgments

The sample of $Li_3Lu_3Te_2O_{12}$ was prepared by Richard MacManus. We would also like to acknowledge the assistance of Dr. Ron Smith in carrying out the neutron diffraction experiments at ISIS and the Science and Technology Facilitates Council for providing this beamtime. EJC would like to thank the Royal Society for provision of a University Research Fellowship as well as the EPSRC and the University of Strathclyde for funding.

References

[1] V. Thangadurai, H. Kaack, W.J.F. Weppner, J. Am. Ceram. Soc. 86 (2003) 437.
[2] E.J. Cussen, J. Mater. Chem. 20 (2010) 5167.
[3] E.J. Cussen, Chem. Commun. (2006) 412.
[4] M.P. O'Callaghan, E.J. Cussen, Chem. Commun. 20 (2007) 2048.
[5] R. Murugan, V. Thangadurai, W. Weppner, Angew. Chem. Int. Ed. 46 (2007) 7778.
[6] J. Percival, E. Kendrick, R.I. Smith, P.R. Slater, Dalton Trans. (2009) 5177.
[7] J. Awaka, N. Kijima, H. Hayakawa, J. Akimoto, J. Solid State Chem. 182 (2009) 2046.
[8] J. Percival, E. Kendrick, P.R. Slater, Mater. Res. Bull. 43 (2008) 765.
[9] R. Murugan, W. Weppner, P. Schmid-Beurmann, V. Thangadurai, Mater. Res. Bull. 43 (2008) 2579.
[10] E.J. Cussen, T.W.S. Yip, J. Solid State Chem. 180 (2007) 1832.
[11] M.P. O'Callaghan, E.J. Cussen, Solid State Sci. 10 (2008) 390.
[12] M.P. O'Callaghan, D.R. Lynham, G.Z. Chen, E.J. Cussen, Chem. Mater. 18 (2006) 4681.
[13] H.M. Rietveld, J. Appl. Crystallogr. 2 (1969) 65.
[14] A.C. Larson, R.B. von Dreele, General Structure Analysis System (GSAS), Los Alamos National Laboratories, Los Alamos, NM, 1990.
[15] V. Thangadurai, W. Weppner, Adv. Funct. Mater. 15 (2005) 107.
[16] J. Percival, P.R. Slater, Solid State Commun. 142 (2007) 355.
[17] R.D. Shannon, Acta Cryst. A 32 (1976) 751.
[18] J. Percival, D. Apperley, P.R. Slater, Solid State Ionics 179 (2008) 1693.
[19] L. Van Wüllen, T. Echelmeyer, H.-W. Meyer, D. Wilmer, PCCP 9 (2007) 3298.
[20] M.A. Meyers, A. Mishra, D.J. Benson, Prog. Mater Sci. 51 (2006) 427.
[21] C. Demetry, X.L. Shi, Solid State Ionics 118 (1999) 271.
[22] M.P. O'Callaghan, J.T. Titman, G.Z. Chen, E.J. Cussen, Chem. Mater. 20 (2008) 2360.